DeepBeam – A Machine Learning Framework For Tuning The Primary Electron Beam of The PRIMO Monte Carlo Software

Zbisław Tabor (tabor.zbislaw@gmail.com)
AGH University of Science and Technology: Akademia Gorniczo-Hutnicza imienia Stanislawa Staszica w Krakowie https://orcid.org/0000-0002-9688-9718
Damian Kabat
Maria Skłodowska Curie Memorial Cancer Centre and Institute of Oncology Krakow Department of Medical Physics: Centrum Onkologii-Instytut im Marii Sklodowskiej-Curie Oddzial w Krakowie Zaklad Fizyki Medycznej
Michael Waligórski
Tadeusz Kosciuszko Cracow University of Technology: Politechnika Krakowska im Tadeusza Kosciuszki

Research

Keywords: Machine learning, deep learning, Monte Carlo, beam simulation, quality assurance, QA, quality control QC, PCA-principal component analysis, support vector regression

Posted Date: April 26th, 2021

DOI: https://doi.org/10.21203/rs.3.rs-425712/v1

Version of Record: A version of this preprint was published at Radiation Oncology on June 29th, 2021. See the published version at https://doi.org/10.1186/s13014-021-01847-w.

DeepBeam – a machine learning framework for tuning the primary electron beam of the PRIMO Monte Carlo software

[(1)]Zbisław Tabor, [(2)]Damian Kabat, [(3)]Michael Waligórski

[(1)] AGH University of Science and Technology,
Al. Adama Mickiewicza 30, 30-059 Kraków, Poland, tabor.zbislaw@gmail.com
[(2)] Maria Sklodowska-Curie National Research Institute of Oncology Krakow Branch,
Garncarska 11, 31-115 Krakow, Poland, z5kabat@cyfronet.pl
[(3)] Cracow University of Technology, Podchorążych 1, 30-084 Kraków, Poland,
z5waligo@cyf-kr.edu.pl

Author to whom correspondence should be addressed: Zbisław Tabor,
tabor.zbislaw@gmail.com

Abstract

Background

Any Monte Carlo simulation of dose delivery using medical accelerator-generated megavolt photon beams begins by simulating electrons of the primary electron beam interacting with a target. Because the electron beam characteristics of any single accelerator are unique and generally unknown, an appropriate model of an electron beam must be assumed before MC

simulations can be run. The purpose of the present study is to develop a flexible framework with suitable regression models for estimating parameters of the model of primary electron beam in simulators of medical linear accelerators, basing on real reference dose profiles measured in a water phantom.

Methods

All simulations were run using PRIMO MC simulator. Two regression models for estimating the parameters of the simulated primary electron beam, both based on machine learning, were developed. The first model applies Principal Component Analysis to measured dose profiles in order to extract principal features of the shapes of the these profiles. The PCA-obtained features are then used by Support Vector Regressors to estimate the parameters of the model of the electron beam. The second model, based on deep learning, consists of a set of encoders processing measured dose profiles, followed by a sequence of fully connected layers acting together, which solve the regression problem of estimating values of the electron beam parameters directly from the measured dose profiles. Results of the regression are then used to reconstruct the dose profiles, basing on the PCA model. Agreement between the measured and reconstructed profiles can be further improved by an optimization procedure resulting in the final estimates of the parameters of the model of the primary electron beam. These final estimates are then used to determine dose profiles in MC simulations.

Results

Analysed were a set of actually measured (real) dose profiles of 6 MV beams from a real Varian 2300 C/D accelerator, a set of simulated training profiles, and a separate set of simulated testing profiles, both generated for a range of parameters of the primary electron beam of the Varian 2300 C/D PRIMO simulator. Application of the two-stage procedure based on regression followed by reconstruction-based minimization of the difference between measured (real) and reconstructed profiles resulted in achieving consistent estimates of

electron beam parameters and in a very good agreement between the measured and simulated photon beam profiles.

Conclusions

The proposed framework is a readily applicable and customizable tool which may be applied in tuning virtual primary electron beams of Monte Carlo simulators of linear accelerators. The codes, training and test data, together with some trained models and readout procedures, are freely available at the site: https://github.com/taborzbislaw/DeepBeam.

Key words: Machine learning, deep learning, Monte Carlo, beam simulation, quality assurance, QA, quality control QC, PCA-principal component analysis, support vector regression.

I. Introduction

External photon beam therapy (EBT) is nowadays the most common cancer radiotherapy modality. The key factors which determine the success of EBT are correct and accurate treatment therapy planning and quality assurance procedures prior to delivery of the therapeutic dose. Designing a therapy plan is a multi-dimensional optimization problem. The therapy planning system (TPS) designs therapy plan to match the therapy goals within specified clinical tolerances. Only after assuring that these goals are met, may the quality assurance procedures of dose delivery be implemented and the patient treated.

The dose calculation algorithms are the true engines of all TPS systems. The first generation Pencil Beam Convolution (PBC) algorithm calculates the delivered dose by convoluting the ionizing radiation field intensity (or fluence) with pencil beam kernels and by applying subsequent corrections for patient tissue heterogeneity, as based on CT data [1]. The next generation Anisotropic Analytical Algorithm (AAA) is a semi-analytical model which also uses pencil beams. The AAA pencil beams are determined using the photon beam data of a linac. Heterogeneity corrections in the AAA algorithm also account for scattered radiation [2]. The ACUROSE XB (AXB) algorithm solves deterministically a coupled system of linear Boltzmann transport equations to model the transport of ionizing radiation through a homogeneous medium, subsequently applying heterogeneity corrections and explicitly modelling the interaction of radiation with matter, basing on patient CT data [3]. As all the aforementioned algorithms are only approximations, they must be thoroughly tested against a reference gold standard.

In modern radiotherapy, Monte Carlo (MC)-calculated dose distributions are currently the primary reference tool for verifying other dose-calculation methods, or for benchmarking commercial dose calculation algorithms. Ultimately, MC modelling is expected to replace the current approximate algorithms in therapy planning [4]. It is generally accepted that Monte

Carlo simulation of dose delivery is the most reliable and accurate method of representing the real aspects of calculating dose distributions [5]. This is because MC modelling incorporates all aspects of photon and electron transport in generally heterogeneous media. However, while being potentially very accurate and extremely valuable in gaining thorough understanding of all phenomena related to dose deposition in various media, it is also a very challenging task [4]. This is due not only to the high computational effort required by MC modelling, but also because of the tuning process which must be carefully implemented to match MC-calculated doses and doses measured under controlled conditions. Tuninig of a MC simulator of a medical accelerator involves three basic steps, namely geometry tuning, virtual electron beam tuning, and dose unit calibration.

Any MC simulation of dose delivery by megavolt photon beams from a medical linear accelerator commences by simulating the primary beam of high-energy electrons which leave the acceleration tube of the linac with a well-specified energy of several MeV impinging a carefully designed tungsten cone target to generate megavolt photons via bremsstrahlung. The spatial distribution of dose delivered by the thus generated photon beam to a water phantom or to the patient's tumour volume, crucially depends on the characteristics of the primary electron beam. To MC-model the details of photon beam production and of its distribution, scattering and shaping by various collimators and instruments located in the head of the linac, their exact geometry configuration, material composition and construction of the head of a commercially produced medical linear accelerator must be known in great detail. Given the high precision of manufacture and assembly of all mechanical parts of a modern linac, its head geometry and construction details are not expected to significantly vary within a production line of accelerators of a given type from a given manufacturer. This considerably facilitates implementation of geometry considerations in MC calculations when simulating a given model of a commercially produced linear accelerator. Yet, the primary electron beam

characteristics of any individual accelerator are unique. Moreover, the characteristics of their primary electron beams may vary not only between linacs of the same type, but may also vary in time within the same accelerator, due to ageing effects [6-8]. Unfortunately, the geometry and spectra of the primary electron beam are neither known exactly nor easily measurable, except by quite specialized equipment, which is not readily available in a typical clinical radiotherapy environment [9,10].

For this reason, to run MC simulations, an appropriate model of the electron beam must be designed, which includes a model of its electron energy spectrum and model of its spatial distribution. Typically, no less than four parameters are needed to characterise a MC-simulated electron beam of a medical linear accelerator – namely the mean energy of electrons in the beam, the full width at half-maximum of the electron energy spectrum in the beam, the radial distribution of electrons in the beam, and the angular divergence of this beam. Clearly, in order to generate a clinically realistic MC simulation of dose delivery from any individual accelerator, the parameters of the model of the electron beam must be determined specifically for that accelerator [11].

For above-discussed reasons, availability of a well-defined and realistically executable procedure of specifying the MC model of the primary electron beam in an individual linear accelerator is of major importance in the subsequent application of MC-based modelling of clinical procedures using this particular accelerator. Notably, parameters of a MC model of the electron beam of a linac can only be determined indirectly by analysing a number of depth and lateral dose-profiles measured in specified conditions, best in a standard water phantom.

Due to the fundamental importance of this issue, several studies have been published proposing various experimental setups and methods of such analysis [6-9,11-18]. In the study of Almberg et al. [9] an algorithm is proposed to determine values of two parameters (nominal

energy and spot size) of the primary electron beam model, basing on depth and lateral photon beam profiles measured for three fields: 2x2, 10x10, and 20x20 cm2. The MC profiles are calculated for preselected values of nominal energies and spot sizes. The authors propose an ad hoc cost function, calculated from a range of hand-crafted features extracted from profiles, to select between some preselected nominal energy and spot size values those which minimize the cost function. The algorithm, iterating over preselected values, finds values of only two of the four model parameters. The tuning procedure proposed in the study of Pena et al. [12] is aimed at determining three parameters (the nominal energy, spot size, and angular divergence) of the primary electron beam model, basing on a depth and a penumbra profile for the 5x5 cm2 field and three lateral profiles for four fields: 5x5, 10x10, 20x20, and 40x40 cm2. The MC profiles are also calculated for preselected values of nominal energies and an arbitrarily fixed values of spot size and angular divergence. In the first step, the authors, using these fixed angular divergence and spot size values and applying a figure of merit, search for an optimal energy, iterating over MC results. Only the first step of this tuning procedure is formalized, because in the next step, after fixing the energy parameter to the value found in the previous step, an optimal spot size is searched for by trial and error, comparing measured and simulated penumbra for a 5x5 cm2 field. In the last step, the value of the angular divergence parameter is searched for, also by trial and error, using lateral profiles. The last two steps require an extensive MC simulation effort while being based on a trial-and-error approach. Other studies of [13-18] are also based on a trial-and-error approach which, while being computationally demanding, offers no systematic procedure for estimating parameter values in the applied model of the primary electron beam.

It follows that in the published papers describing tuning the model of the primary electron beam, ad hoc approaches are primarily used. In most cases a trial-and-error approach has been adopted. Other approaches rely on of searching for the beam model parameters using

various figures of merit, over a predefined set of parameters for which MC results have been pre-computed. Within some hybrid approaches, the value of one of the model parameters is found by searching over a set of preselected values while values of the remaining parameters are found by trial and error - which again requires extensive MC simulation.

The published studies generally share common feature – they lack any phenomenological model enabling the values of primary electron beam parameters to be estimated directly from the measured dose profiles. They also suffer from specific, often quite demanding requirements with respect to experimental equipment and measurement procedures. As different measurement devices and different dosimetry procedures are typically used at various clinical centres, relaxing such constraints is highly desirable.

In contrast to such studies, we propose a flexible framework, termed DeepBeam, such that its user may collect the profile data using dosimetry tools and protocols at her/his disposal and select the profiles to be measured according to her/his best experience. Then, a regression model is created which can be directly and routinely used to estimate the parameters of the model of the primary electron beam. The proposed framework, apart from tuning electron beams of Monte Carlo simulators of real linear accelerators and, possibly, consecutive in silica designs of radiotherapy procedures, may also be applied in routine quality assurance of an operating linear accelerator – not only to verify its beam stability via dose profile analysis, but also to indicate which of the beam parameters had likely changed and by how much. The complete code of this framework and the data used for training the regression models are freely available at https://github.com/taborzbislaw/DeepBeam .

II. Material and methods

II.1. The MC simulator and sources of data

While the proposed framework for tuning primary electron beams of MC simulators of linear accelerators can be used for any such simulator, the present study is based on data generated by the PRIMO simulator, version 0.1.5.1307 [19] (www.primoproject.net). PRIMO is a freely-distributed application used for simulating dose delivery during radiotherapy [8,18,19]. It is based on the PENELOPE 2011 [20] general purpose Monte Carlo engine and allows simulation of dose delivery to be performed for some other linear accelerator models, based on their geometry, as provided by their manufacturers. This last feature is especially important, as details of accelerator geometry are usually confidential and may not be available from the manufacturer, even upon request. Hence, using PRIMO, attention could be focussed on the primary goal of designing a framework for tuning the electron beam of this simulator without undue concern with simulation details related to the physics, materials or the geometry configuration of the simulated accelerator system.

All simulations were run using the PRIMO Varian Clinac 2300 C/D simulator operating in photon mode at a nominal energy of 6 MV. Electron beam simulation in PRIMO is configured by specifying values of four beam parameters: E - the initial electron beam energy (in MeV), σ_E - the full-width-at-half-maximum (FWHM) of the primary beam energy distribution (in MeV), s - the focal spot FWHM (in cm), and α - the angular beam divergence (in degrees). The developed framework should however be readily adaptable if different primary beam parameters were specified in the PRIMO simulator, or if other MC simulators of linear accelerators were applied.

II.1.1. Simulated input data

To generate training data for the machine learning framework, the simulations were run for a total of 300 tuples (E, σ_E, s, α) within the set S such that:

$$S = \{(E, \sigma_E, s, \alpha): E \in \{5.6,5.8,6.0,6.2,6.4\}, \sigma_E \in \{0.0,0.5,1.0\}, \\ s \in \{0.0,0.1,0.2,0.3,0.4\}, \alpha \in \{0,1,2,3\}\} \quad (1)$$

At the first simulation stage, 10^8 histories (a history corresponds to a single electron of the virtual primary beam) were simulated for each tuple (E, σ_E, s, α) and the phase-space file (PSF) above the secondary collimators was saved for further purposes. At this first stage, the splitting roulette variance reduction technique [21] was used with the size of the splitting region set to the largest region, i.e. to the 40×40 cm^2 field. The saved PSFs were then used to simulate dose delivery to a homogeneous cubic water phantom for three fields: 3×3 cm^2, 10×10 cm^2, and 30×30 cm^2. The size of the phantom was set to 50×50×50 cm^3. The doses in the phantom were tallied within a regular grid of 0.5×0.5×0.5 cm^3 voxels. The respective faces of the phantom were set parallel to the respective main axes of the coordinate frame of reference of the accelerator. The main axis of the phantom coincided with the photon beam axis. The source-to-surface distance (SSD) was set at 100 cm, the isocentre being located at the front surface of the phantom. Splitting in the water phantom was selected as the variance reduction method [21] at this simulation stage, with a splitting factor of 300. The uncertainty of the dose values tallied in the water phantom always remained within 1.5%. The calculated 3D spatial distribution of doses within the phantom was saved to a text file, separately for each tuple (E, σ_E, s, α) and for each field. A total of 900 3D dose files were collected. Each 3D dose file contained 10^6 dose values measured at (x,y,z) coordinates given by the following coordinate ranges:

$$x \in \{-25 + 0.25 + 0.5 * i, i = 1 \ldots 100\} \\ y \in \{-25 + 0.25 + 0.5 * j, j = 1 \ldots 100\}, \quad (2) \\ z \in \{0.25 + 0.5 * k, k = 1 \ldots 100\}$$

where the z axis is parallel to the radiation field axis. To generate testing data for the machine learning framework, the simulations were run further for 25 tuples (E, σ_E, s, α) with primary beam parameters sampled as follows:

$$\begin{matrix} E \in \{5.65 + i \cdot 0.05, i = 0 \ldots 14\} \setminus \{5.8, 6.0, 6.2\} \\ \sigma_E \in \{0.1 + i \cdot 0.1, i = 0 \ldots 8\} \setminus \{0.5\} \\ s \in \{0.05 + i * 0.1, i = 0 \ldots 3\} \\ \alpha \in \{0.5 + i * 0.25, i = 0 \ldots 9\} \setminus \{1, 2\} \end{matrix} . \quad (3)$$

Applying the above sampling scheme, it was assured that the primary electron beam parameters (E, σ_E, s, α) in the testing set never coincided with parameters used for generating the training set, and consequently, that the electron beam parameters for the testing set were well separated from the electron beam parameter selected for training.

All simulations were run using the PlGrid infrastructure (Prometheus grid, https://kdm.cyfronet.pl/portal/Main_page) and required a total real time of about 2.5 months. During the simulation period 12 Prometheus nodes run the PRIMO software, each node equipped with two Intel Xeon E5-2680v3 processors, 24 cores in total, and 128 GB RAM. The simulation of a single case, i.e., of three fields for a single tuple (E, σ_E, s, α), required about 40 CPU hours. As the operating system installed on the nodes is Linux CentOS 7, while PRIMO is a Windows application, *wine* software (https://www.winehq.org/) was installed and configured in order to use PRIMO in graphic mode under Linux exactly as if Windows were the operating system.

II.1.2. Measured input data

Dose profiles were measured in water for the 6 MV photon beam of a clinically exploited Clinac 2300C/D medical accelerator at the Krakow Branch of the National Research Institute of Oncology. A PTW MP3 Water Phantom and PTW Markus Type 23343 and PTW Semiflex

Type 31010 ionization chambers were used for dosimetry. PTW Mephysto software was applied for data collection. Three experimental setups of dose profile measurements were arranged, as described in more detail in the Results section.

II.2. Applied models and computational framework

The task to solve is a regression problem, i.e., given dose profiles in a water phantom, the parameters (E, σ_E, s, α) of the primary electron beam are to be estimated. To prepare training and test data, each 3D dose spatial distribution was normalized to the dose value calculated along the photon beam axis at the depth of maximum (D_{max} = 1.4 cm), which was then set to 100% (such normalization is not essential if not implemented in a clinical measurement system). Next, from each 3D dose file six profiles were extracted: one depth profile along the axis of the radiation field, and five lateral profiles at depths: 1.4 cm, 5 cm, 10 cm, 20 cm, and 30 cm. To match the resolution of the simulated profiles and the typical spatial resolution of clinical dosimetry systems (usually 1 mm), linear interpolation was applied to the tallied simulated doses during profile extraction. Additionally, as PRIMO assumes the electron beam spot to be of circular shape, the lateral dose profiles extracted from the 3D dose files consisted of averages over two perpendicular lateral dose profiles over the x and y directions. Such averaging is not a necessary condition and may be skipped if a more complex, e.g., elliptic, electron spot shape is assumed by the accelerator simulator.

The extracted dose profiles (18 profiles for each tuple (E, σ_E, s, α)) represent a reasonable maximum set $Prof_{MAX}$ of dose profiles to be used in the proposed machine learning framework. Moreover, the extracted depth dose profiles span the range of $z \in$ <0.3 cm, 49.7 cm>, while all the extracted lateral dose profiles span the range of $x \in$ <-24.7 cm, 24.7 cm>, i.e., the maximum ranges for the geometry of the simulated water phantom and for the spatial resolution of the grid of tallied dose values.

The proposed framework is customizable, meaning that any subset of the dose profiles can be selected from the complete set of dose profiles to match the needs of an individual user. The ranges over which the profiles are measured can also be arbitrarily selected to match the measurement ranges of real profiles. For example, the user may decide to build her/his regression model which predicts the parameters of the model of the electron beam (E, σ_E, s, α) from the depth dose profiles and from lateral dose profiles at 10 cm depth, all collected for 10×10 cm^2 and 30×30 cm^2 fields, depth dose profiles measured up to 35 cm, and lateral dose profiles measured over the ranges between -10 cm to +10 cm and between -20 cm to +20 cm, for 10×10 cm^2 and 30×30 cm^2 fields, respectively. Given these user-defined constraints the framework finds the optimum regression model, as described in the following sections.

II.2.1. PCA + SVR regression model

Let $Prof = \{Prof_1, Prof_2, \ldots, Prof_n\}$ represent a user-selected subset of $Prof_{MAX}$. A user-selected spatial range $Range_i$ is associated with each $Prof_i$ ($Range_i$ would typically be the user-dependent spatial range over which $Prof_i$ is measured under clinical settings). Each subscript i corresponds to a unique field size and a unique dose profile type (either depth or lateral, at one of the five depths: D_{max}=1.4 cm, 5 cm, 10 cm, 20 cm, or 30 cm).

As each dose profile $Prof_i$ is sampled within a given spatial resolution (usually 1 mm), it may be considered a 1D vector of some dimensionality (dependent of the sampling resolution and the sampling range $Range_i$). The regression task which is to be solved can be formulated as follows:

$$Par = f_{Par}\left(Prof_1, Prof_{2,\ldots}, Prof_n\right) + \epsilon_{Par}, \quad (4)$$

where *Par* is any element of the tuple (E, σ_E, s, α), f_{Par} is the regression function and ε_{Par} is the residual term. The components of each $Prof_i$ are however strongly correlated as they represent dose values measured at neighbouring spatial locations. For this reason, the model given by Eq. (4) may not be very effective, as the set of explanatory variables (arguments of f_{Par}) contains a high contribution of redundant information.

To resolve this redundancy problem dimensionality reduction is applied. Typically, dose profiles are specified by applying some ad-hoc features, such as width at half maximum, width of penumbra regions, "wing heights" in lateral profiles, etc. Here, rather than rely on such hand-crafted features, Principal Component Analysis (PCA) is applied to the analysed profiles [22]. PCA will then find uncorrelated features which form a linear combination of the original features (dose values). Moreover, each PCA feature is assigned a percentage of the total variance of profile shapes it explains. As demonstrated in what follows, three most important PCA features usually explain over 98% of the variability of shapes of the training dose profiles. PCA reduces the dimensionality of the space of explanatory variables by a factor of 10^2 – the final set of features consists of $3n$ elements (explanatory variables) - three features for each profile $Prof_i$ in *Prof*. The learnt PCA models were saved in respective files (a separate PCA model $M_{PCA,i}$ file for each index i) and subsequently used at the stage of model testing.

Clearly, for each i - index there are 300 training profiles $\{Prof_{i,1}, Prof_{i,2,\ldots}, Prof_{i,300}\}$ corresponding to 300 different tuples $\{(E, \sigma_E, s, \alpha)_1, (E, \sigma_E, s, \alpha)_2, \ldots, (E, \sigma_E, s, \alpha)_{300}\}$ and a single PCA model $M_{PCA,i}$ which extracts three features $(F_{i,1}, F_{i,2}, F_{i,3})_k$ from $Prof_{i,k}$. Hence, the regression problem, after dimensionality reduction, becomes:

$$Par = f_{PAR}^{PCA}\left(F_{1,1}, F_{1,2}, F_{1,3}, F_{2,1}, F_{2,2}, F_{2,3}, \ldots, F_{n,1}, F_{n,2}, F_{n,3}\right) + \epsilon_{PCA}, \quad (5)$$

where *Par* is any element of the tuple (E, σ_E, s, α), f_{PAR}^{PCA} is the PCA-based regression function and ε_{PCA} is the residual term. To learn the regression functions, the following training set, *Tr*, was applied:

$$Tr = \left\{(E, \sigma_E, s, \alpha)_K, \left\{\left(F_{1,1}, F_{1,2}, F_{1,3}\right)_K, \left(F_{2,1}, F_{2,2}, F_{2,3}\right)_K, \ldots, \left(F_{n,1}, F_{n,2}, F_{n,3}\right)_K\right\}, K = 1..300\right\}. \quad (6)$$

Support Vector Regression (SVR) with rbf kernel was selected as the regressor [23] though other options are also available. The best regression models were selected using a 5-fold cross validation run on *Tr*. After training, four f_{PAR}^{PCA} regressors were obtained, one per E, σ_E, s, and α. The regression models were saved to files and subsequently used in testing.

II.2.2. The Deep Learning regression model

The processing pipeline described in the previous section consists of two separate steps: feature extraction, and training of four regressors. In the current section an end-to-end regression model is described which, during training, learns both dose profile data representation and regression functions simultaneously for all primary beam parameters (E, σ_E, s, α). The model presented here is based on deep learning. The architecture of the deep learning (DL) model is outlined in **Fig. 1**.

The architecture is designed to follow the same processing steps as the approach described in the previous section. In short, each $Prof_i$ in *Prof* is a separate input for the DL model and is processed by a separate encoder block. Each encoder block consists of a few convolution blocks. Each convolution block consists of two 1D convolutions (filter size equal to 3, number of filters equal to 16, 32, 64, etc. in the consecutive convolution blocks, ReLU

activation) followed by a MaxPool1D layer which reduces the size of the data by a factor of two. The number L of convolution blocks in each encoder block is selected based on the length N of the input of this block, according to the formula $L = \text{int}(\log_2 N/3)$, i.e., the number of features learnt by any encoder block cannot be less than 3. Each encoder block ends with 1D convolution with a single filter of unit size. The outputs of the encoder blocks are then concatenated to form a 1D vector of features (in analogy to PCA features). This feature vector is then processed by two fully connected layers of size 100 and ReLU activation. The output of the last fully connected layer is next fed into the final fully connected layer with four outputs and no activation. These outputs are expected to deliver estimates of E, σ_E, s, and α.

The training data Tr_{DL} for the DL model is:

$$Tr_{DL} = \{(E, \sigma_E, s, \alpha)_K, \{Prof_{1,K}, Prof_{2,K}, \ldots, Prof_{n,K}\}, K = 1 \ldots 300\} \quad . \tag{7}$$

The model is trained for 300 epochs using the Adam optimizer and a constant learning rate equal to 0.0001. The loss function selected for this regression problem was mean square error between the model outputs and ground truth data. A 20% portion of the training set was randomly selected for model validation. The best model found during training was saved to a file and used in subsequent testing.

II.2.3. Testing the models

At the stage of model testing, the testing profiles were fed at the input of either the PCA+SVR or DL models. The PCA+SVR model first extracts the features from the testing profiles based on PCA models learnt on the training set. These test features are then processed by SVR regressors which return the predicted values of E, σ_E, s, and α. In the case of the DL model the raw testing profiles are fed at the input of the DL model which returns the predicted values

of E, σ_E, s, and α. The true and predicted values of E, σ_E, s, and α are then compared using correlation analysis and linear regression.

II.2.4. Optimizing the solution with profiles reconstructed from regression results

The regression results can be further improved by minimizing the difference between the actual profiles being fed at the input of regressors and profiles reconstructed from the regression results. In particular, the parameters of the model of the primary electron beam for the training set *Tr* (Eq. (6)) have the form of a regular grid *S*, defined in Eq. (1), embedded within a 4D hypercube *H*. With every node *Q* of *S* associated are PCA features corresponding to the dose profiles determined for primary electron beam model parameters $(E, \sigma_E, s, \alpha)_Q$ assigned to *Q*. The regressions return a point $P = (E, \sigma_E, s, \alpha)_{PRED}$ within *H* (see Fig. 2 for a 2D example). Consecutively, using interpolation, PCA features corresponding to *P* may be determined, and next an inverse PCA transform applied to them in order to reconstruct profiles from the results of regression models $(E, \sigma_E, s, \alpha)_{PRED}$. Thus, for each $Prof_i$ in *Prof* a reconstructed profile $RecProf_i(P)$ obtains, which in general differs from $Prof_i$. This difference can then be further minimized using one of several optimization methods, with $(E, \sigma_E, s, \alpha)_{PRED}$ as the starting point for such minimization. Namely, beginning with $P = (E, \sigma_E, s, \alpha)_{PRED}$, $P_{MIN}=(E, \sigma_E, s, \alpha)_{MIN}$ is sought, such that:

$$P_{MIN} = \underset{P \in H}{argmin} \sum_{i=1}^{n} w_i \, \| Prof_i - RecProf_i(P) \|^2, \qquad (8)$$

where w_i is the weight assigned to the *i*-th profile. In the experiments all w_i were set to unity but in general the user may set these according to her/his actual needs. The minimization problem defined in Eq. (8) was solved using the SLSQP method [24].

II.2.5. Applied software

All models were implemented in Python 3.6.10. The *scipy* library (version 1.5.2) was used to implement regression models using PCA and SVR. The same library was used to run interpolation over 3D dose distributions to extract dose profiles, optimization of the regression results and profile reconstruction from regression results. The DL model was implemented using the *keras* (version 2.3.1) library. All codes, pretrained models, as well as training and testing data, are freely available at https://github.com/taborzbislaw/DeepBeam .

III Results

III.1. Analysis of simulated training data

Detailed analysis of simulated training data formed the basis for model design decisions and aided in selecting the best hyperparameters for the developed model. Following these decisions, a final verification of the performance of the model was performed using only test data. Thus, in accordance with the fair model selection principle, test data were never used in model fine-tuning.

The first issue considered was what number of PCA features extracted from the profiles explains what fraction of the variability in the shapes of profiles. Results are shown in **Fig. 3a** separately for three analysed fields (3x3 cm^2, 10x10 cm^2 and 30x30 cm^2) as averages over six profiles extracted from the simulated 3D dose distributions for each of these three fields (depth profile and five lateral profiles at depths D_{max} = 1.4 cm, 5 cm, 10 cm, 20 cm, and 30 cm). The error bars represent standard deviations of the values of explained variance, calculated over the six profiles of these three fields. Clearly, three PCA features suffice in explaining most of the variability of the shapes of profiles, so any further increase of PCA features above that number would not offer much in terms of added benefit.

Results shown in **Fig. 3b** illustrate the relative contributions that each of the three most important PCA features introduce in explaining the variance of profile shape. It is

445 evident that the first PCA feature explains most of the variation in the depth profile (ID=1).
446 The contributions offered by consecutive PCA features in explaining the overall variation in
447 the shapes of lateral profiles increase with increasing depth at which these lateral profiles are
448 extracted. It follows from this figure that use of lateral profiles extracted at larger depths
449 offers more benefit in model predictions, as the variability of their shapes is richer (i.e., the
450 contribution of higher PCA modes to the shape of the final profile is then more pronounced).
451 Effectively, more information about the primary electron beam may be encoded in such
452 profiles at larger depths.

453 The impact of the three major PCA features on the shape of dose profiles is shown in
454 **Fig. 4** for two selected profiles (10x10 cm^2 lateral profile at 30 cm depth - upper panels, and
455 10x10 cm^2 depth profile – lower panels). Here, changes with respect to the mean profile
456 shapes when varying any one of the three most important PCA features are shown. The PCA
457 features of mean profiles are all equal to zero. Profiles marked in this figure as "Negative
458 feature" have only the first, second, or third PCA feature negative in plots within the left,
459 middle, or right panels, respectively. Similarly, profiles marked as "Positive feature" have
460 only the first, second, or third PCA feature positive in respective left, middle, or right panels.

461 The coefficient of determination between ground truth and predicted values of energy,
462 spot size, and angular divergence is shown in **Fig. 5**. The coefficient of determination was
463 calculated for held-out parts of the full training set, in accordance with cross-valdation
464 approach. Results presented in this figure are obtained for regressors trained on different
465 numbers of profiles of any of the three fields: 3x3 cm^2, 10x10 cm^2, and 30x30 cm^2. For
466 example, in the case of the number of profiles of each field being equal to one, only depth
467 profiles of the three fields were used for regressor training. For the number of profiles of each
468 field equal to two, depth profiles and lateral profiles at 1.4 cm depth of these three fields were
469 used for regressor training. It follows from the results shown in this figure that a total of six

profiles (one depth and one lateral), that is two from each of three (3x3 cm^2, 10x10 cm^2 and 30x30 cm^2) fields, would suffice in precisely predicting the values of E, s, and α.

Note that in **Fig. 5** predictions of the FWHM of the primary beam energy distribution, σ_E, have not been presented, as it was not possible to train a regressor to precisely predict the value of σ_E. The effect of varying the value of σ_E on the shapes of the profiles was noted to be very small – below 2%, in line with the noise level, which is the likely cause of lack of success in training regressors to predict the value of the parameter which represents the energy distribution of the primary beam. Thus, only E, s, and α (energy, spot size, and angular divergence) were further considered in the analysis.

The coefficient of determination between ground truth and predicted values of energy, spot size, and angular divergence for a limited selection of profiles (depth, lateral at depth of D_{max}=1.4 cm and lateral at depth of 10 cm) and a varied number of fields for these profiles was also analysed. Application of a total of six profiles - one depth profile and two lateral profile, and any two of three fields (3x3 cm^2, 10x10 cm^2, or 30x30 cm^2) would be sufficient in obtaining precise predictions of E, s, and α values. It appears however that three profiles extracted from a single field (except for the 3x3 cm^2 field alone), would also be sufficient to precisely determine the values of primary electron beam parameters E, s, and α, with a coefficient of determination above 0.98.

Considering the above-discussed results obtained using training, the final design decision was made to train regressors based on PCA features extracted from a total of six profiles, i.e., three profiles (depth, lateral at D_{max}=1.4 cm depth and lateral at 10 cm depth) of two field sizes (10x10 cm^2 and 30x30 cm^2).

The testing results for the PCA+SVR model are shown in **Fig. 6**. Models trained on the training data were applied to previously unseen testing data and the predicted values of primary beam parameters compared to the ground truth data, i.e., the values of primary beam

parameters applied in the generation of simulated profiles. Notably, the values of the coefficient of determination for the testing data were only slightly lower than those obtained for the training data - implying that the regressors were not overfitted. Also shown in this figure are best-fitted linear regression lines to demonstrate the precision with which the model is able to predict the primary beam parameters. The slopes of these regression lines are all close to 1.0. The prediction errors were estimated as values of standard deviation of the difference between the true and predicted values of the primary electron beam parameter, and were equal to 0.03 MeV, 0.007 cm, and 0.13^{O} for *E*, s, and α, respectively.

The testing results for the deep learning model trained on the same set of profiles as those used for the PCA+SVR model are shown in **Fig. 7**. The results for the deep learning model are slightly inferior to those obtained for the PCA+SVR model which is not surprising, since the deep model was trained only on 300 sets of profiles, which may not be sufficient for a deep learning task. Further refinements would certainly be possible, however in that case more data would need to be generated. Yet, as demonstrated in the next section, both models offer good starting points for optimization-based estimates of the parameters of a model of the primary electron beam from clinical measurements, leading to virtually the same final results. The prediction errors for the deep model were equal to 0.065 MeV, 0.023 cm, and 0.21^{O} for *E*, s, and α, respectively.

Discrepancies between the slopes of the best fit lines and the ideal 1.0 value are due to the noise present in the training data, which, although being relatively low (1.5%) is however higher than that in real measurements. Decreasing the noise level to 0.5% would however increase the computation time by a factor of 10 which is unrealistic in view of the computational expense. The optimization procedure which follows the regression, as described in the previous section, resolves this issue.

III.2. Analysis of clinical data

The developed framework was used to find the values of primary electron beam parameters which could best reproduce real profiles measured using the 6 MV photon beam of a Clinac 2300C/D medical accelerator in a PTW MP3 Water Phantom. The applied input fields and profiles, obtained beam parameters, and mean errors of the reconstructed dose distributions against those measured, for three cases of experimental setups discussed below, are gathered in **Table 1**. The measured and reconstructed profiles for the respective sets of input profiles in each of these three cases are compared in **Fig. 8**.

Table 1. Results of SVR regression and deep model analysis of clinical profile data.

Case ID	**Applied Fields**	**Applied Profiles**	**Beam parameters**			**Mean absolute error between measured and reconstructed profiles [%]**
			SVR regression E_{PRED}, s_{PRED}, a_{PRED}	**DL regression E_{PRED}, s_{PRED}, a_{PRED}**	**Final estimation E_{FINAL}, s_{FINAL}, a_{FINAL}**	
1	3x3 cm^2	Depth profile	5.54 MeV, 0.0 cm, 1.97^O	6.02 MeV, 0.0 cm, 2.35^O	5.86 MeV, 0.0 cm, 2.44^O	0.33
		Lateral at Dmax				0.94
	10x10 cm^2	Depth profile				0.50
		Lateral at Dmax				1.03
	30x30 cm^2	Lateral at Dmax				0.90
2	10x10 cm^2	Depth profile	5.47 MeV, 0.23 cm, 2.08^O	5.50 MeV, 0.18 cm, 2.41^O	5.60 MeV, 0.25 cm, 2.39^O	0.33
		Lateral at 10 cm depth				0.41
	30x30 cm^2	Lateral at Dmax				0.49
		Lateral at 10 cm depth				0.26
3	10x10 cm^2	Depth profile	5.43 MeV, 0.24 cm, 1.95^O	5.62 MeV, 0.27 cm, 2.47^O	5.60 MeV, 0.24 cm, 2.41^O	0.35
		Lateral at Dmax				0.75
		Lateral at 10 cm depth				0.40

	30x30 cm^2	Depth profile				0.26
		Lateral at Dmax				0.43
		Lateral at 10 cm depth				0.20

Table legend: The results for three experimental setups (Cases 1-3)) are reported in the table. The applied input fields and profiles are shown in columns 2 and 3. Values of PCA+SVR or DL- predicted beam parameters are shown in in columns 4 and 5. The mean absolute differences between the measured profiles and profiles reconstructed using final estimation parameters are shown in the last column.

Three experimental design cases were investigated, where different sets of measured profiles (as shown in the second and third columns of Table 1) were used as input. In each of the three cases, the models were trained on a set of training profiles corresponding to those measured, after suitable adjustment of the ranges of the training profiles. Following this training, the measured profiles were then input to the trained PCA+SVR or DL models to obtain the values of the parameters of the model of the primary electron beam, E_{PRED}, s_{PRED}, and α_{PRED} , shown in the fourth and fifth columns of Table 1, respectively. Because there was no possibility to train a regressor for predicting the value of σ_E, σ_E = 0.50 MeV was consistently used throughout. These initial predictions were next fed as input to the reconstruction-based minimization procedure. After optimizing these predicted values for either model, usually identical (or very similar) sets of finally estimated parameter values: E_{FINAL}, s_{FINAL}, and α_{FINAL} , shown in column 5 of Table 1, were obtained. These finally estimated electron beam model parameters values were then used to calculate the reconstructed dose profiles. The measured and reconstructed profiles in each of the three experimental cases are compared in **Fig. 8**. The mean values of absolute differences between the measured and reconstructed profiles are given in the last column of **Table 1**.

The first set of measured profiles *(Case 1)* consisted of five profiles: two depth profiles and three lateral profiles, one of which was measured at the depth of D_{max}=1.4 cm, as listed in Table 1. The depth profiles were measured to a depth of 35 cm while the ranges of measurement of lateral profiles were adjusted to the field size. The ranges of training data for this set of profiles were adjusted to the ranges of real measurements prior to being applied to train the PCA+SVR or DL models. The returned sets of values of the predicted parameters from either model are listed in columns 4 and 5 of Table 1, for the PCA+SVR and DL models, respectively. As mentioned earlier, σ_E=0.50 MeV was consistently used. A reconstruction-based minimization procedure was then applied to these predicted values, resulting in identical values of final estimates, E_{FINAL}, s_{FINAL}, and α_{FINAL} for either model, as listed in column 6 of Table 1. The mean absolute differences between the measured profiles and profiles reconstructed using these final parameter values (column 7 in Table 1) are shown in the last column of Table 1. The measured and reconstructed profiles for this case are shown in **Fig. 8a.**

The second set of measurement profiles *(Case 2)* consisted of one depth profile and three lateral profiles, one of which was measured at depth D_{max}, listed in column 2 of Table 1. The depth profile was measured to a depth of 30 cm while the ranges of measurement of lateral profiles were adjusted to the field size. The regression models were retrained for this set of profiles and returned the initial guesses for the primary beam parameter values shown in column 4 of Table 1. After optimization, the final prediction values shown in column 6 of Table 1 were obtained. The deep (DL) model retrained for this set of profiles was then applied to predict values of electron beam parameters using this set of measurement profiles. The prediction results of the DL model are listed in column 5 of Table 1. After optimization, the same set of final prediction values as those from the PCA+SVR model was obtained, i.e., those shown in column 6 of Table 1. The mean absolute differences between the profiles:

576 measured and reconstructed using these final beam parameters are shown in the last columns
577 of Table 1. The measured and reconstructed profiles for this case are shown in **Fig. 8b.**

578 Finally, the third set of measurement profiles *(Case 3)* consisted of six profiles: a
579 depth profile and two lateral profiles, both at D_{max} depth. The depth profile was measured to a
580 depth of 30 cm while the ranges of measurement of lateral profiles were adjusted to the field
581 size. The regression models were retrained for this set of profiles and returned an initial guess
582 for the primary beam parameter values shown in column 4 of Table 1. After optimization, the
583 final predictions for the PCA+SVR model are shown in column 6 of Table 1. The DL model
584 was also trained for this set of profiles and the values of predicted parameters of the primary
585 electron beam are listed in column 5 of Table 1. After repeated optimization of the same set,
586 again the set of finally predicted parameter values from the DL model and that from the
587 PCA+SVR optimized models, were identical (column 6 in Table 1) The mean absolute
588 differences between the profiles measured and those reconstructed using these last parameter
589 values are shown in the last column of Table 1. The measured and reconstructed profiles for
590 this case are shown in **Fig. 8c.**

591 Commenting generally on the results obtained, one should note the remarkably
592 consistent estimates of beam parameters obtained using either the PCA+SVR or the deep
593 learning models, and the excellent agreement between the reconstructed and measured
594 profiles, especially using the set of measured profiles and fields in the Case 3 study. However,
595 even in the Case 1 study, the somewhat higher discrepancies observed at the borders of the
596 lateral fields are to be expected. Over such regions of high dose gradients, higher uncertainties
597 may be due to measurement uncertainties, to averaging of input data by the phantom software
598 or to averaging of data in the training profiles, all affecting the quality of reconstructed
599 profiles over such regions. The excellent agreement between the reconstructed and real

profiles is confirmed by the low values of mean absolute errors displayed in column 6 of Table 1 in most cases ranging around 0.5% and exceeding 1% only once.

While the selection of measured profiles appears to be the best for the Case 3 experimental setup where large fields were selected as input, the selection of the input fields and their depth to be applied in simulator tuning should be guided by the expected range of fields to be applied most frequently – hence, e.g., smaller fields should be selected if such fields are expected to be applied more often in clinical work.

While there is a very good agreement between measured and profiles reconstructed from regression results, based on PCA models, a final check of the proposed framework and must be comparison of measured and simulated profiles. To this end, the dose delivery was simulated for 10^9 histories, using the virtual primary electron settings determined for Case 3 measurement experiment. Real profiles and simulated profiles for this case are compared in **Fig. 9**.

IV. Discussions

Cancer radiotherapy using external photon beams, often termed *conventional radiotherapy* is the most frequently applied form of radiotherapy world-wide. However, contemporary elements of this type of radiotherapy – the linear accelerator, the therapy planning software and quality assurance procedures which presently rely on up-to date technology and computer engineering are far from being conventional. Among the critical issues in radiotherapy are the accuracy and repeatability of dose delivery which requires that within the combined system of a medical accelerator, therapy planning and clinical dosimetry, identical absolute dosimetry units are exchanged. Thus, accurate quantitative description of the features of the model of the primary electron beam in a linear accelerator is a major task of critical importance, being immediately related not only to the accuracy of the therapy planning calculations but

625 primarily to the accuracy of dose delivery to the patient - also affected by the correctness of
626 the relative calibration of the therapy planning system. For purposes of routine QA in the
627 clinic it is impossible to measure any parameters of the primary electron beam directly – the
628 only indirect option available is to estimate them on the basis of the dose distribution
629 measured in a clinical water phantom within a well-specified dosimetry procedure.
630 Development of a Monte Carlo-based model to relate specific features of the in-phantom
631 measured dose distributions with values of the basic parameters of the model of the electron
632 beam in a medical accelerator was the prime motivation in this work. Availability of an
633 elsewhere-developed complete MC model of the accelerator, i.e., of the PRIMO Monte Carlo
634 software, and development and successful application of statistical learning technology made
635 it possible to accomplish this task.

636 Ideally, for the solution of such a task to be of practical utility, it should be delivered
637 as a model which accepts at its input a well-defined assembly of measured profiles, returning
638 estimated values of the parameters characterizing the primary electron beam of a given
639 accelerator, together with dose profiles reconstructed basing on these estimated parameters.
640 Clearly, any discrepancy between the measured and the reconstructed profiles should be as
641 small as possible, which depends on the data used to train the learning models. Customization
642 of model inputs is a major obstacle, as medical physics departments often apply different
643 measurement tools, phantoms or measurement protocols. For these reasons, any specifically
644 defined procedure which requires measurements of a strictly limited and predefined set of
645 profiles according to a unique protocol would not be a solution likely to be universally
646 accepted.

647 The solution presented in this study is flexible and readily usable. Based on Monte
648 Carlo simulation data, a set of models was developed which extract features from a user-
649 defined collection of dose profiles to estimate primary electron beam model parameters from

650 such features and returns reconstructed profiles for comparison with those measured and used
651 as input. Estimation of primary electron beam model parameters involves two steps – an
652 initial guess and optimization of the solution based on a model of the features of the measured
653 profiles. In contrast to all the work published so far, the characteristics of the dose profile
654 shapes and the regression functions are both machine-learned and collected in a data-
655 dependent manner. Neither hand-crafted shape features nor ad-hoc regression functions need
656 to be applied, these being replaced by a well-established background of statistical learning.
657 The two models developed in this work – one based on PCA feature extraction and SVR
658 regression and another, based on end-to-end deep-learning which simultaneously learns to
659 represent the shapes of the dose profiles and to apply the most suitable regression functions –
660 are the proposed solution. Such a solution will support several different experimental
661 arrangements, offering optimum regression models for any such arrangement. By studying a
662 few experimental cases, the effect of the selection of the experimental setup on the accuracy
663 of parameter estimation has been demonstrated and discussed.

664 As was already mentioned, estimation of the primary electron beam model parameters
665 involves two steps, the first of which is an initial guess made by a regression model. In
666 principle, this initial guess could be made without any such model - merely by a brute force
667 search over all collected profiles for a set of profiles that best fit the analysed profiles. The
668 second stage of estimation, which is based on reconstruction-based minimization, requires
669 that techniques be developed to effectively represent the shape of the measured profiles - as
670 introduced in the present work. It should also be noted that a brute force search delivers no
671 explanatory power, in contrast to regression models introduced in the present study. In
672 particular, regression models deliver an association between explanatory and explaining
673 variables – for example, given a regression model it can be inferred in what manner will any
674 specific changes of primary electron beam model parameters influence the shapes of the

675 resulting dose profiles. This is the general advantage of regression models over any brute
676 force search strategies, which is why regression models are widely used in statistical data
677 analysis.

678 The developed framework was tested using both simulated and real data. The tests
679 based on simulated data demonstrated that the coefficient of determination of true primary
680 beam parameters from dose profiles varies from around 92% for angular beam divergence to
681 97% for mean energy of the simulated electron beam. It was not possible to train the
682 developed model to predict the FWHM of energy spectrum of primary electrons, implying
683 that this particular beam parameter does not seriously affect the shapes of dose profiles, at
684 least for the cases studied in this work.

685 The presented framework has been made freely available together with the simulation
686 data used for training the models. Model training and testing stages do not require extensive
687 computation resources. Using any up-to-date PC with no graphic card support, the PCA+SVR
688 models can be trained within a few seconds and prediction takes no longer than a second. The
689 training of deep learning models usually requires about ten hours of an average CPU.
690 However, testing the deep models takes no longer than testing the PCA+SVR model.

691 The presented framework can be readily adapted to individual requirements, perhaps
692 guided by the availability of profile sets prepared for QA purposes, or by ease of
693 measurement. Dose data could also be supplied by dose distributions measured by detectors
694 other than ionization chambers, e.g., dye films, especially over regions of high dose gradient.
695 Indeed, for any selection of profiles which the user intends to apply in determining values of
696 parameters of the primary electron beam models, only a few lines of the configuration code
697 need to be changed to indicate such user-specified selection. Then, the regression models
698 must be retrained, which takes only a few seconds with no user intervention, except for
699 running the code. Following this training run, the estimation of electron beam model

parameters and reconstruction of profiles from estimation results can be executed – this requiring a few more seconds, provided that the measured doses are read by a script. Three examples of such procedures for reading measured doses from text files have also been provided in the freely available repository at https://github.com/taborzbislaw/DeepBeam .

Conclusion

The purpose of the present study was to develop a flexible framework with suitable regression models for estimating parameters of the model of primary electron beam in simulators of medical linear accelerators, basing on real reference dose profiles measured in a water phantom. The proposed framework is a readily applicable and customizable tool which may be applied in tuning virtual primary electron beams of Monte Carlo simulators of linear accelerators. The codes, training and test data, together with some trained models and readout procedures, are freely available at the site: https://github.com/taborzbislaw/DeepBeam.

Abbreviations

MC: Monte Carlo, EBT: external beam photon therapy, TPS: therapy planning system, QA: quality assurance, FWHM: full width at half maximum, PCA: Principal Component Analysis, SVR: Support Vector Regression, DL: deep learning

Acknowledgements

This research was supported by PLGrid Infrastructure. The authors wish to thank Mr. Łukasz Flis of the ACC Cyfronet AGH for his invaluable help in handling computations on the Prometheus grid.

Author's contributions

ZT conceived the work, conducted all the simulations, performed the subsequent analyses, wrote the manuscript and revised it. DK conducted the measurements, wrote the manuscript and revised it. MW wrote the manuscript and revised it.

Funding

This study was supported by the Foundation for Polish Science under grant POIR.04.04.00-00-15E5/18.

Availability of data and materials

All data and code are available at https://github.com/taborzbislaw/DeepBeam.

Ethics approval and consent to participate

Not applicable.

Consent for publication

All authors consent to the publication.

Competing interests

The author declares that she has no competing interests.

References

[1] Storchi P and Woudstra E. Calculation of the absorbed dose distribution due to irregularly shaped photon beams using pencil beam kernels derived from basic beam data. Phys Med Biol. 1996;41(4):637–56

[2] Ulmer W, Pyyry J, Kaissl W. A 3D photon superposition/convolution algorithm and its foundation on results of Monte Carlo calculations. Phys Med Biol. 2005;50(8):1767–90

[3] Failla GA, Wareing T, Archambault Y, Thompson S. Acuros XB advanced dose calculation for the Eclipse treat-ment planning system. Palo Alto, CA: Varian Medical Systems; 2010

[4] Chetty IJ, Curran B, Cygler JE, et al. Report of the AAPM Task Group 105: Issues associated with clinical implementation of Monte Carlo-based photon and electron external beam treatment planning. Med Phys. 2007;34(12):4818–53

[5] Knöös T, Wieslander E, Cozzi L et al. Comparison of dose calculation algorithms for treatment planning in external photon beam therapy for clinical situations. *Phys Med Biol.* 2006; 51(22): 5785-5807.

[6] Björk P, Knöös K, Nilsson P. Influence of initial electron beam characteristics on Monte Carlo calculated absorbed dose distributions for linear accelerator electron beams. *Phys Med Biol*. 2002; 47(22): 4019-4041.

[7] Tzedakis A, Damilakis JE, Mazonakis M, Stratakis J, Varveris H, Gourtsoyiannis N. Influence of initial electron beam parameters on Monte Carlo calculated absorbed dose distributions for radiotherapy photon beams. *Med Phys*. 2004; 31(4): 907-913.

[8] Maskani R, Tahmasebibirgani MJ, HoseiniGhahfarokhi M, Fatahiasl J. Determination of Initial Beam Parameters of Varian 2100 CD LINAC for Various Therapeutic Electrons Using PRIMO. *Asian Pac J Cancer Prev*. 2014; 16(17): 7795-7801.

[9] Pena J, Gonzalez-Castano DM, Gomez F, Sánchez-Doblado F, Hartmann GH. Automatic determination of primary electron beam parameters in Monte Carlo simulation. *Med Phys.* 2007; 34(3): 1076-1084.

[10] Mayles P, Nahum A, Rosenwald JC, Eds. *Handbook of Radiotherapy Physics*. Boca Raton: CRC Press; 2007.

[11] Jiang SB, Kapur A, Ma CM. Electron beam modelling and commissioning for Monte Carlo treatment planning. *Med Phys*. 2000; 27(1): 180-191.

[12] Almberg SS , Frengen J, Kylling A, Lindmo T. Monte Carlo linear accelerator simulation of megavoltage photon beams: independent determination of initial beam parameters. *Med Phys*. 2012; 39(1): 40-47.

[13] Maskani R, Tahmasebibirgani MJ, HoseiniGhahfarokhi M, Fatahiasl J. Determination of Initial Beam Parameters of Varian 2100 CD LINAC for Various Therapeutic Electrons Using PRIMO. *Asian Pac J Cancer Prev*. 2014; 16(17): 7795-7801.

[14] Park H , Choi HJ , Kim JI, Min CH. Analysis of Dose Distribution According to the Initial Electron Beam of the Linear Accelerator: A Monte Carlo Study. *Journal of Radiation Protection and Research.* 2018; 43(1):10-19.

[15] Mohammed M, El Bardouni T, Chakir E, Boukhal H, Saeed M, Ahmed AA. Monte Carlo simulation of Varian Linac for 6 MV photon beam with BEAMnrc code. *Radiation Physics and Chemistry*. 2018; 144 (March 2018): 69–75.

[16] Tugrul T, Erogul O. Determination of initial electron parameters by means of Monte Carlo simulations for the Siemens Artiste Linac 6 MV photon beam. *Reports of Practical Oncology and Radiotherapy*. 2019; 24(4): 331–337.

[17] Najafzadeh M, Hoseini-Ghafarokhi M, Mayn Bolagh RS, Haghparast M, Zarifi S, Nickfarjam A, Farhood A, Chow JCL], J Xray Sci Technol 2019;27(6):1047-1070 Benchmarking of Monte Carlo model of Siemens Oncor® linear accelerator for 18MV photon beam: Determination of initial electron beam parameters

[18] Bacala AM. Linac photon beam fine-tuning in PRIMO using the gamma-index analysis toolkit. *Radiat Oncol*. 2020; 15: 8.

[19] Rodriguez M, Sempau J, Brualla L. PRIMO: a graphical environment for the Monte Carlo simulation of Varian and Elekta linacs. *Strahlentherapie und Onkologie*. 2013; 189(10): 881–886.

[20] Salvat F, Fernández-Varea JM, Sempau J. *PENELOPE 2011—a code system for Monte Carlo simulation of electron and photon transport.* Issy-les-Moulineaux: OECD Nuclear Energy Agency; 2011.

[21] Brualla L, Sauerwein W. On the efficiency of azimuthal and rotational splitting for Monte Carlo simulation of clinical linear accelerators. *Radiat Phys Chem.* 2010; 79 (9): 929–932

[22] Jolliffe IT. *Principal component analysis*, New York: Springer; 2002.

[23] Vapnik VN. *Statistical Learning Theory*. New York: Wiley; 1998.

[24] Kraft D. *A software package for sequential quadratic programming. Tech. Rep. DFVLR-FB 88-28*, Koln: DLR German Aerospace Center — Institute for Flight Mechanics; 1988.

Figure legends

Fig. 1 Scheme of the deep learning regression model architecture.

Fig. 2 Scheme of the method of reconstructing profiles from regression results.

Fig. 3 (a) Fraction of explained variance in the shapes of profiles, versus number of PCA features. The error bars represent standard deviation of the explained variance values, calculated for six profiles of three squared fields (3x3 cm^2, 10x10 cm^2 and 30x30 cm^2); (b) Fraction of profile shape variance explained by the first three features, as averaged over the three squared fields, for six profiles (depth profile: ID=1, and five lateral profiles at depths D_{max}=1.4 cm, 5 cm, 10 cm, 20 cm, and 30 cm, IDs from 2 to 6, respectively).

Fig. 4 Variation in profile shapes in relation to any one of the first three PCA features being either negative or positive (left, middle and right panels) for a 10x10 cm^2, lateral profile at 30 cm depth (upper panels) or for a depth profile of a 10x10 cm^2 field (lower panels). For explanation of "mean shape", "negative feature" and "positive feature" labels, see text.

Fig. 5 Coefficient of determination between ground truth and predicted values of energy, spot size, and angular divergence, for regression based on all of three fields (3x3 cm^2, 10x10 cm^2 and 30x30 cm^2) and a different number of profiles of each field. For further details, see text.

Fig. 6 Testing results for the PCA+SVR model.

Fig. 7 Testing results for the deep learning (DL) model.

Fig. 8 Measured (real) depth and lateral profiles and respective profiles reconstructed using PCA and the finally estimated beam parameters (listed in column 6 of Table 1), for three cases of experimental design. The specification of profiles compared in each panel are listed in columns 2 and 3 of Table 1: (a) Case 1; (b) Case 2; (c) Case 3.

Fig. 9 Measured (real) depth and lateral profiles and respective simulated profiles. The simulation was run for 10^9 histories for experimental settings and virtual primary electron beam profile corresponding to Case 3.

Figures

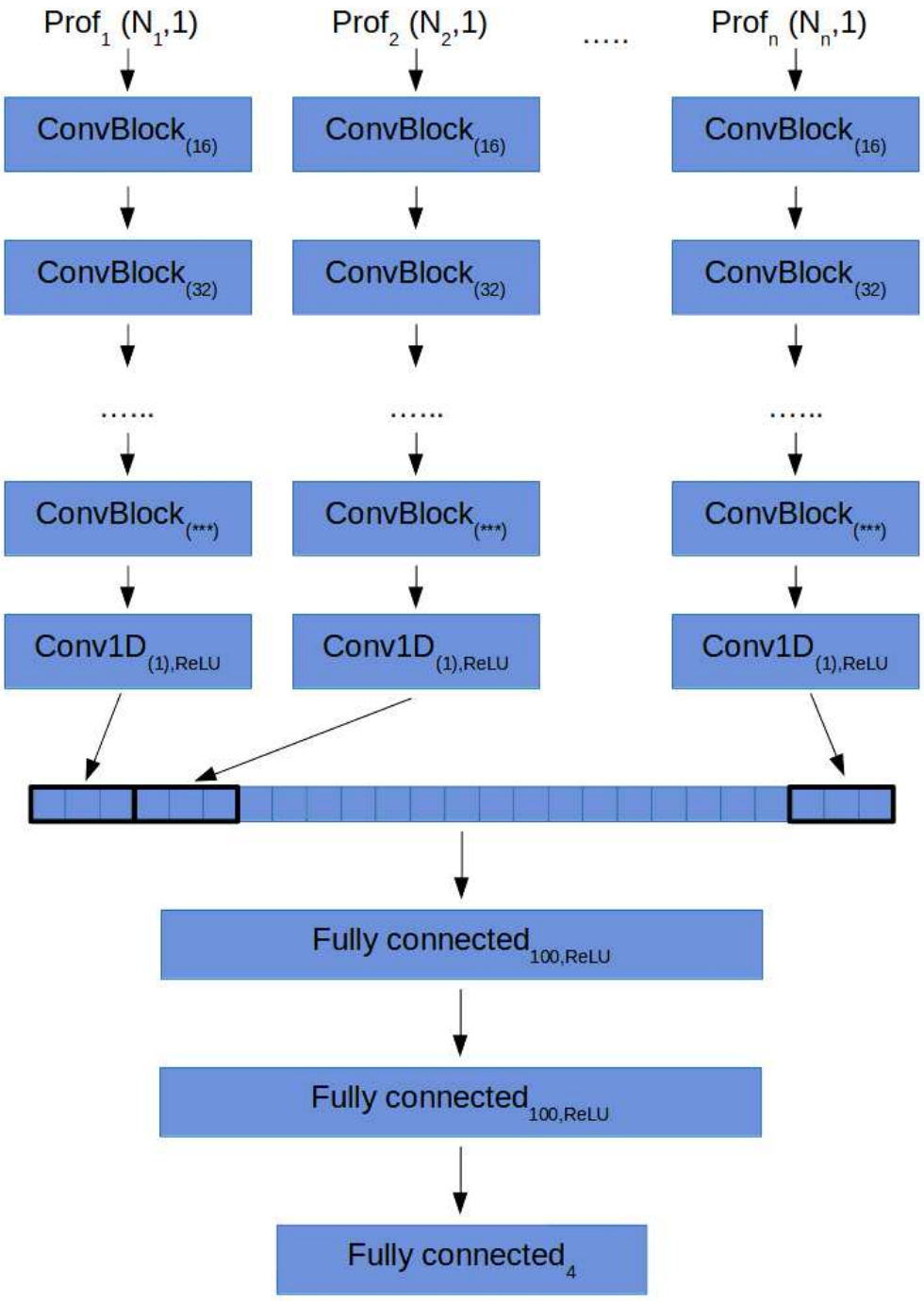

Figure 1

Scheme of the deep learning regression model architecture.

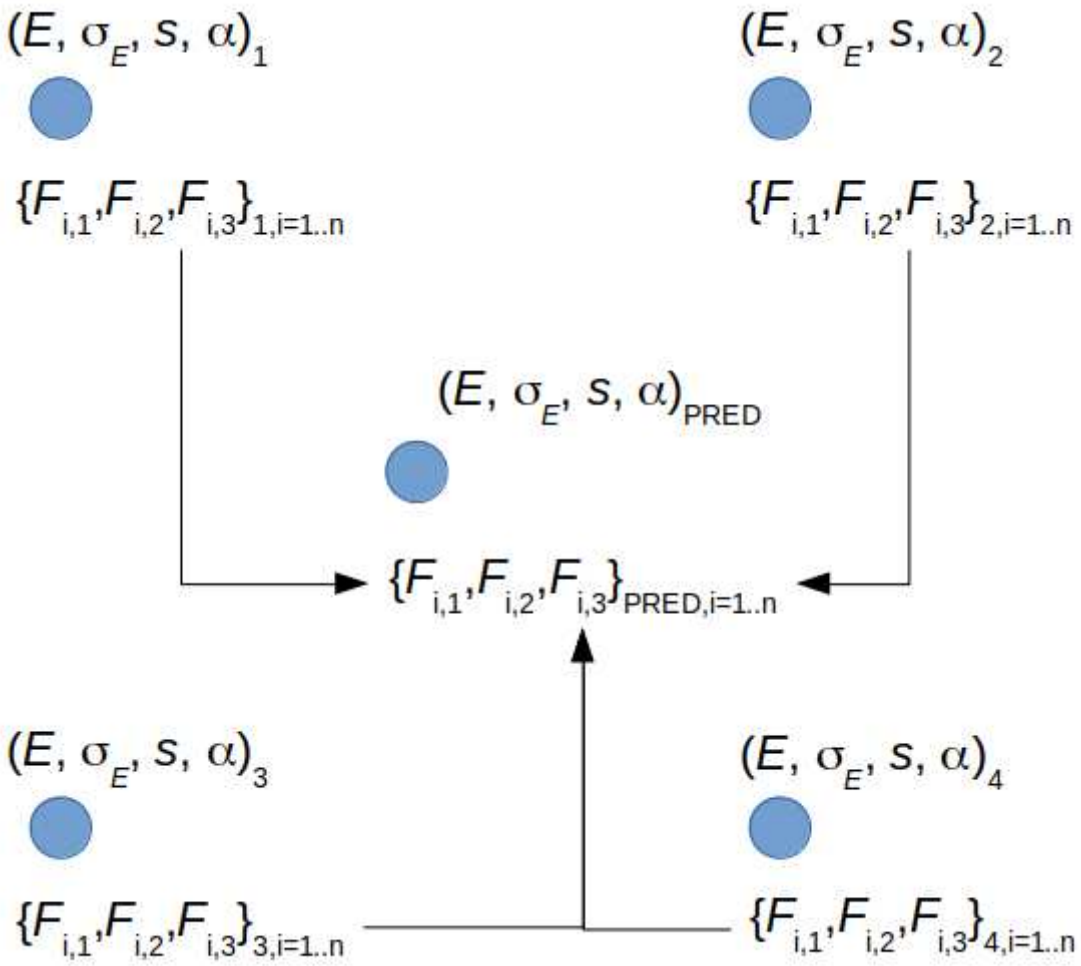

Figure 2

Scheme of the method of reconstructing profiles from regression results.

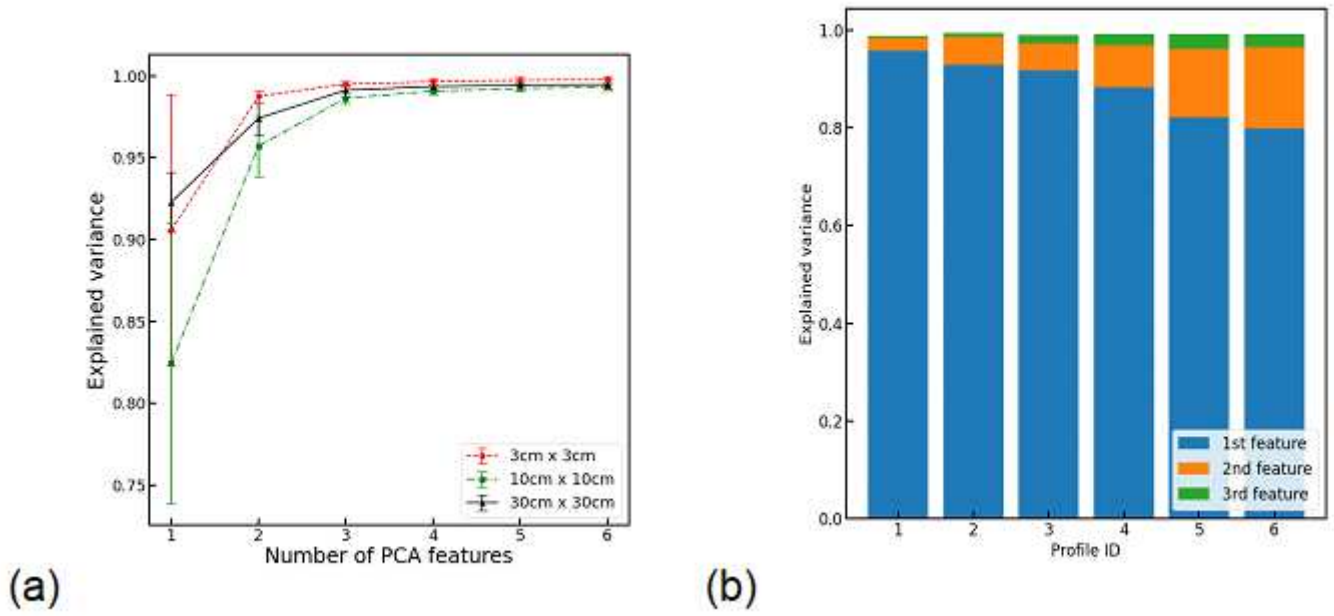

Figure 3

(a) Fraction of explained variance in the shapes of profiles, versus number of PCA features. The error bars represent standard deviation of the explained variance values, calculated for six profiles of three squared fields (3x3 cm2, 10x10 cm2 and 30x30 cm2); (b) Fraction of profile shape variance explained by the first three features, as averaged over the three squared fields, for six profiles (depth profile: ID=1, and five lateral profiles at depths Dmax=1.4 cm, 5 cm, 10 cm, 20 cm, and 30 cm, IDs from 2 to 6, respectively).

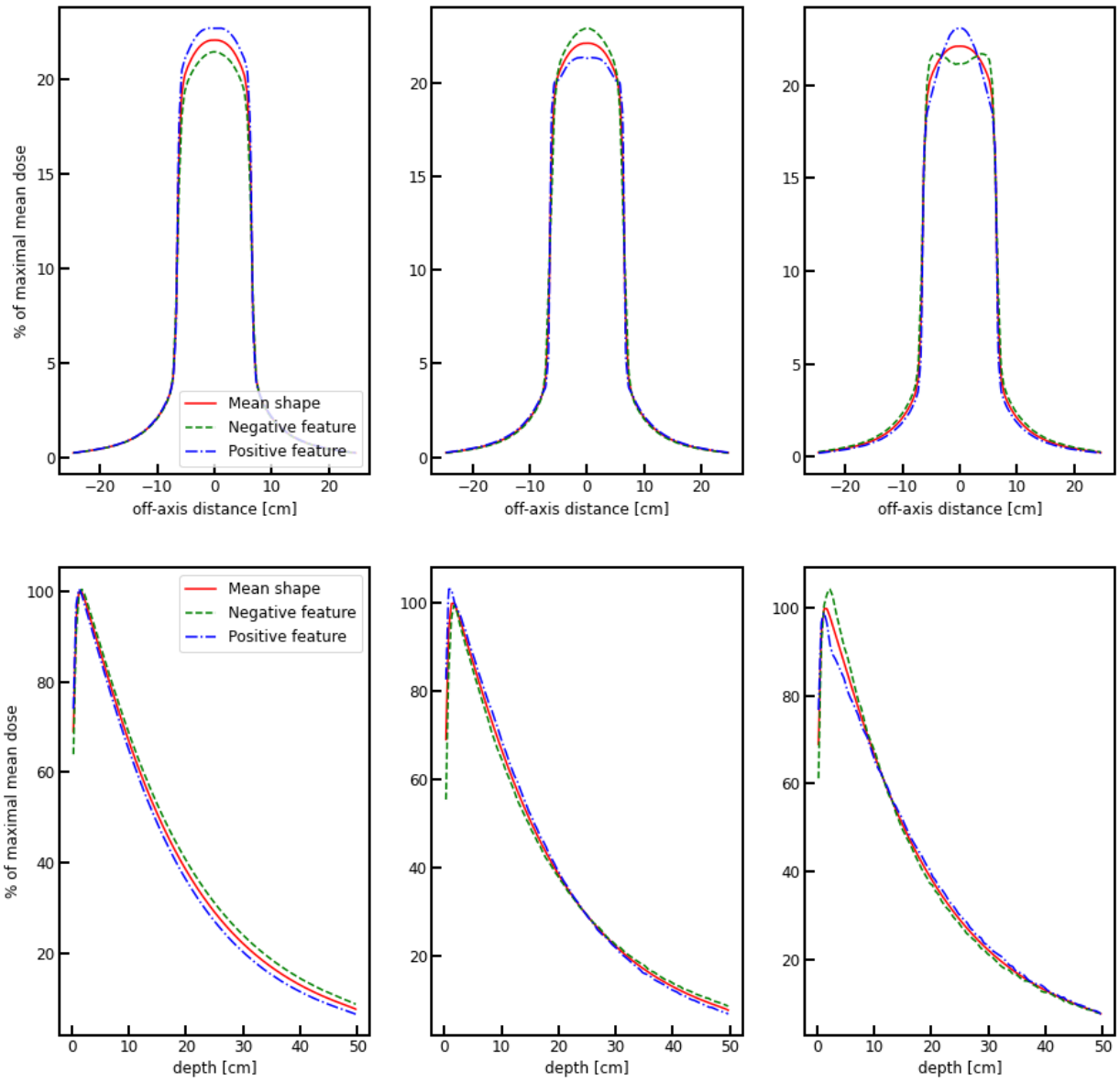

Figure 4

Variation in profile shapes in relation to any one of the first three PCA features being either negative or positive (left, middle and right panels) for a 10x10 cm2, lateral profile at 30 cm depth (upper panels) or for a depth profile of a 10x10 cm2 field (lower panels). For explanation of “mean shape”, “negative feature” and “positive feature” labels, see text.

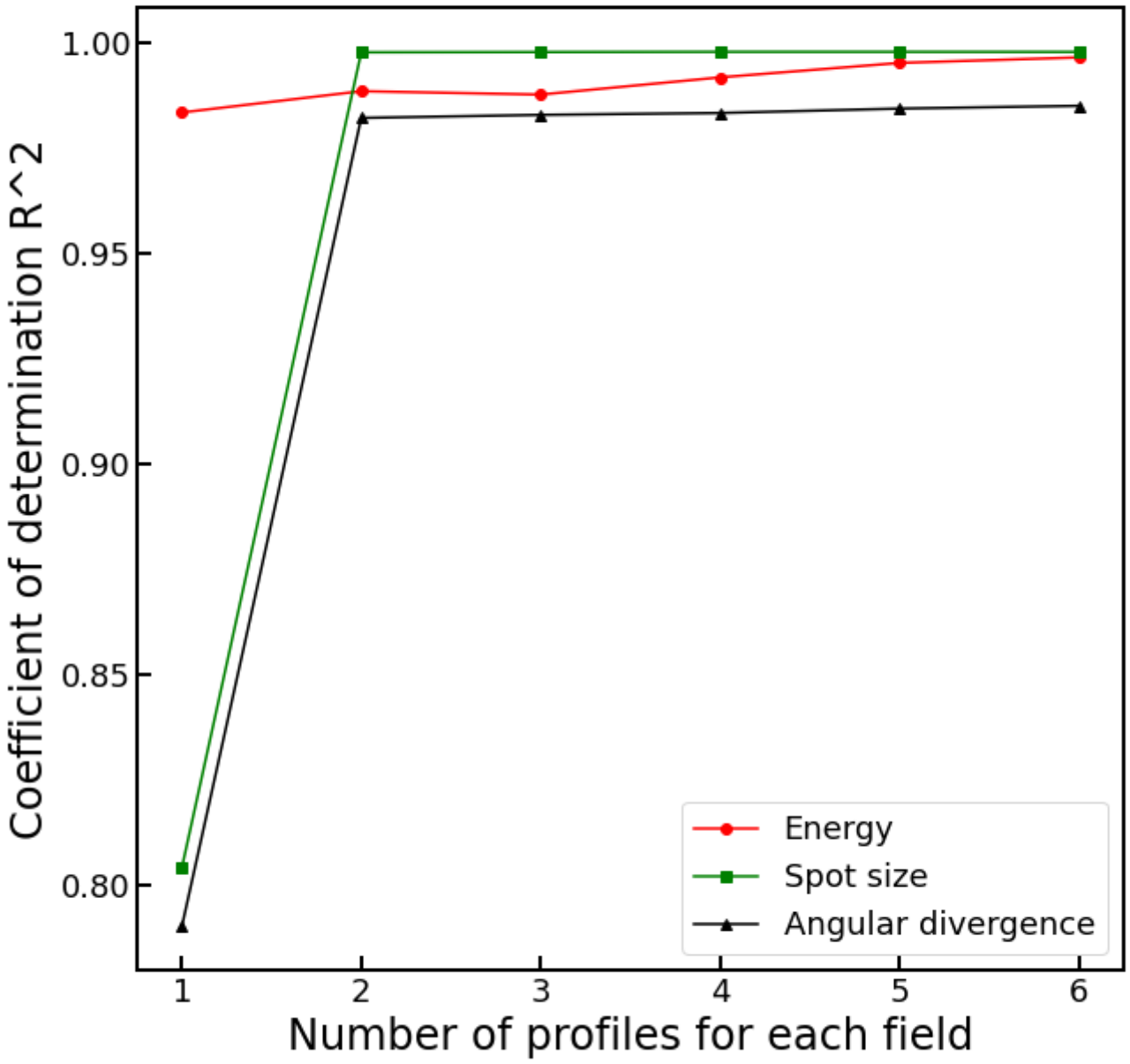

Figure 5

Coefficient of determination between ground truth and predicted values of energy, spot size, and angular divergence, for regression based on all of three fields (3x3 cm2, 10x10 cm2 and 30x30 cm2) and a different number of profiles of each field. For further details, see text.

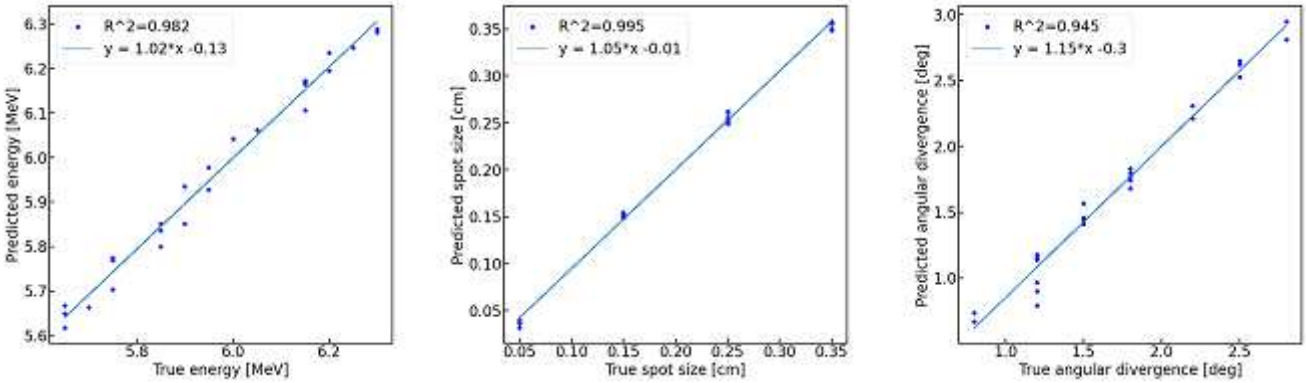

Figure 6

Testing results for the PCA+SVR model.

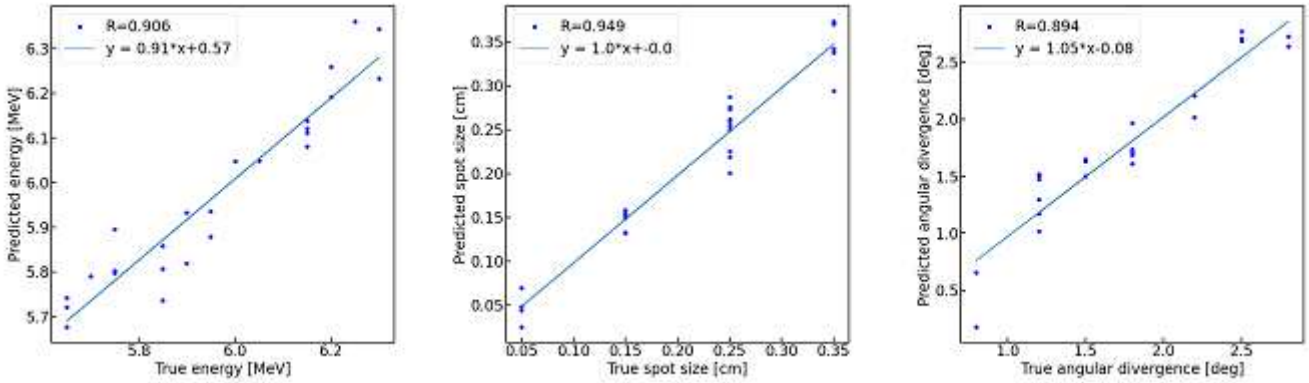

Figure 7

Testing results for the deep learning (DL) model.

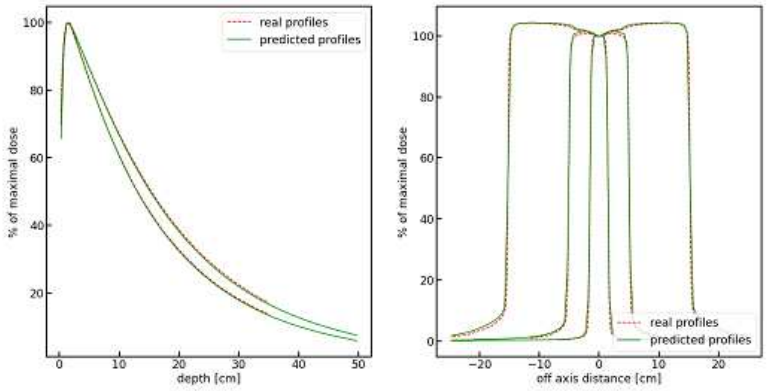

(a)

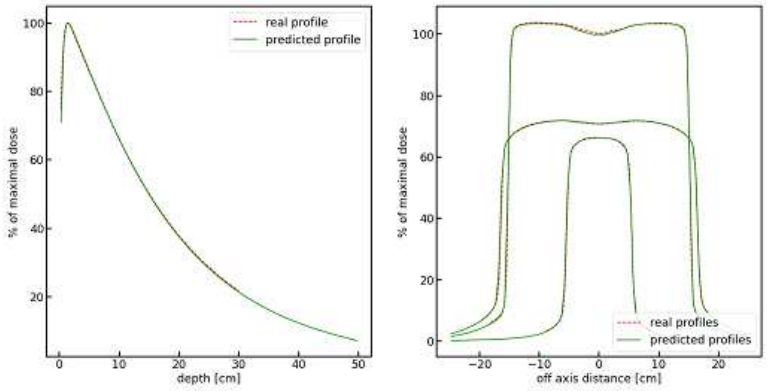

(b)

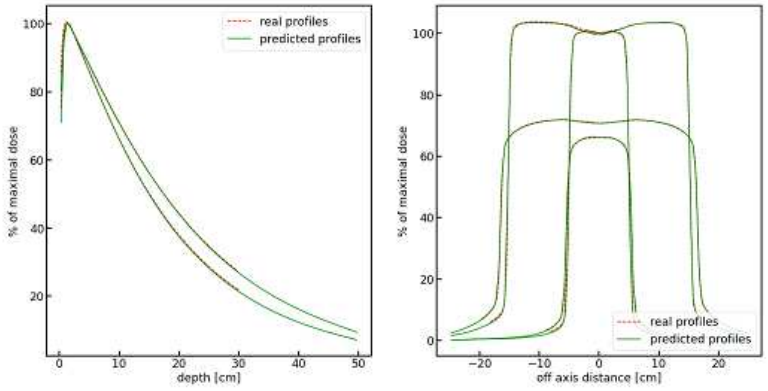

(c)

Figure 8

Measured (real) depth and lateral profiles and respective profiles reconstructed using PCA and the finally estimated beam parameters (listed in column 6 of Table 1), for three cases of experimental design. The specification of profiles compared in each panel are listed in columns 2 and 3 of Table 1: (a) Case 1; (b) Case 2; (c) Case 3.

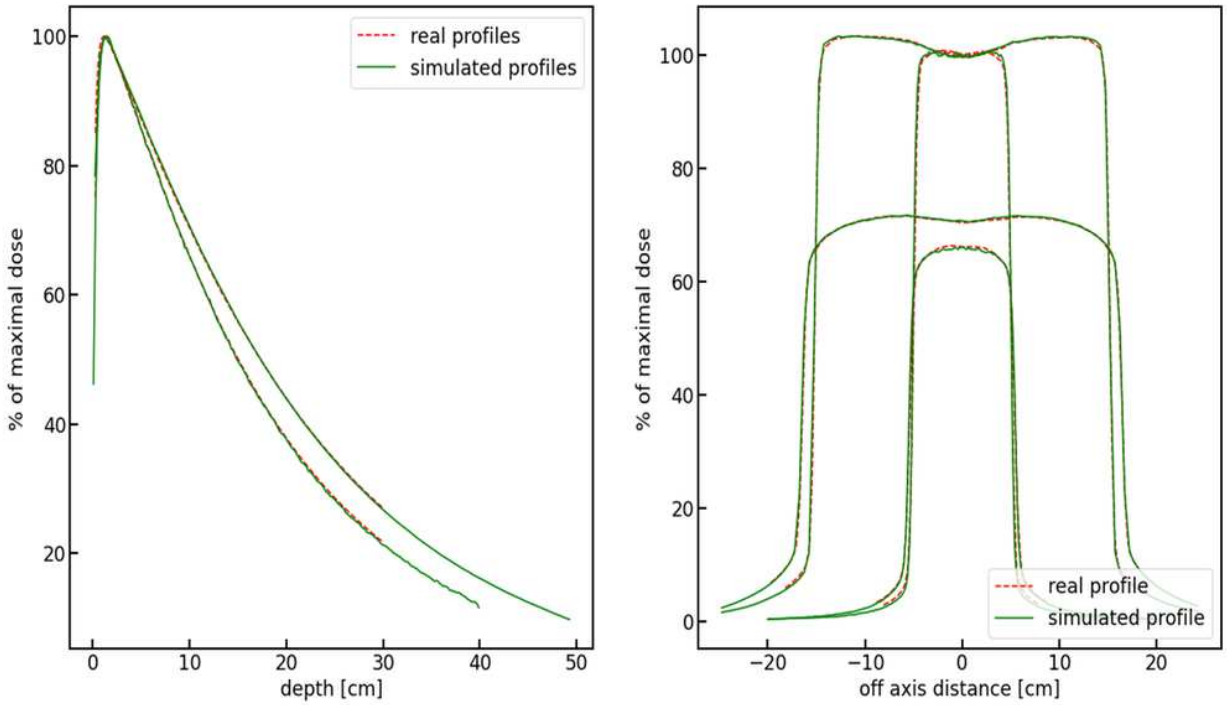

Figure 9

Measured (real) depth and lateral profiles and respective simulated profiles. The simulation was run for 109 histories for experimental settings and virtual primary electron beam profile corresponding to Case 3.